Supplementary Material

Understanding of working mechanism of lithium difluoro(oxalato) borate in Li||NCM85 battery with enhanced cyclic stability

Xuerui Yang[1,2,#], Yaxin Huang[1,#], Jianhui Li[3], Weilin Huang[1], Wen Yang[4], Changquan Wu[2], Shijun Tang[5], Fucheng Ren[5], Zhengliang Gong[5,*], Naigen Zhou[2,*], Yong Yang[1,5,*]

[1] College of Chemistry and Chemical Engineering & Tan Kah Kee Innovation Laboratory (IKKEM), Xiamen University, Fujian, China.
[2]School of Physics and Materials Science, Nanchang University, Nanchang 330031, China.
[3]School of Chemistry, South China Normal University, Guangzhou 510006, China.
[4]College of Chemistry and Chemical Engineering, Jiangxi Province Engineering Research Center of Ecological Chemical Industry, Jiujiang University, Jiujiang 332005, China.
[5]School of Energy, Xiamen University, Xiamen 361102, China.
[#]The authors contributed equally.

Correspondence to: Prof. Zhengliang Gong, College of Energy, Xiamen University, Fujian, China. E-mail: zlgong@xmu.edu.cn; Prof. Naigen Zhou, School of Physics and Materials Science, Nanchang University, Nanchang, China. E-mail: ngzhou@ncu.edu.cn; Prof. Yong Yang, State Key Laboratory of Physical Chemistry of Solid Surfaces, Department of Chemistry and College of Chemistry and Chemical Engineering & Tan Kah Kee Innovation Laboratory (IKKEM), Xiamen University, Fujian, China. E-mail: yyang@xmu.edu.cn

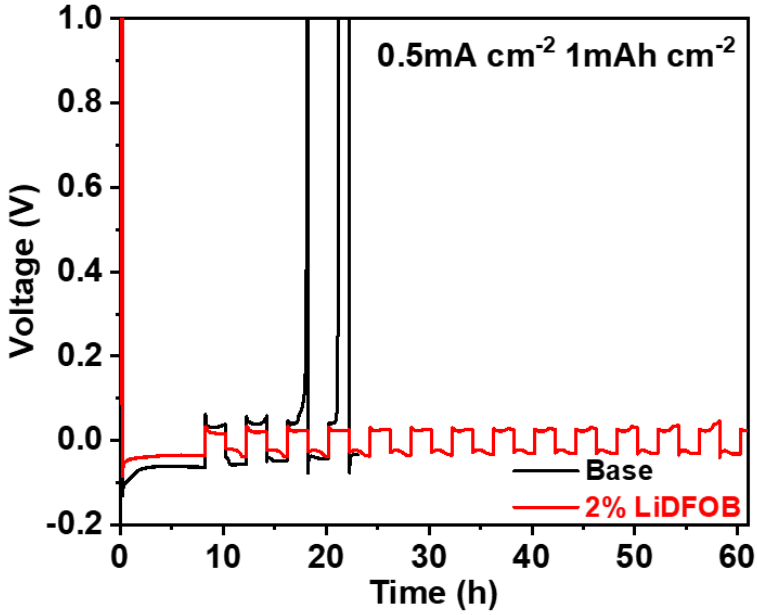

Supplementary Figure 1. Voltage-time profiles of symmetric Li plating/stripping for Li||Cu cells in the electrolyte with and without the LiDFOB additive at 0.5 mA cm^{-2} and 1 mAh cm^{-2} with 4 mAh cm^{-2} Li pre-deposition on the Cu foil substrate.

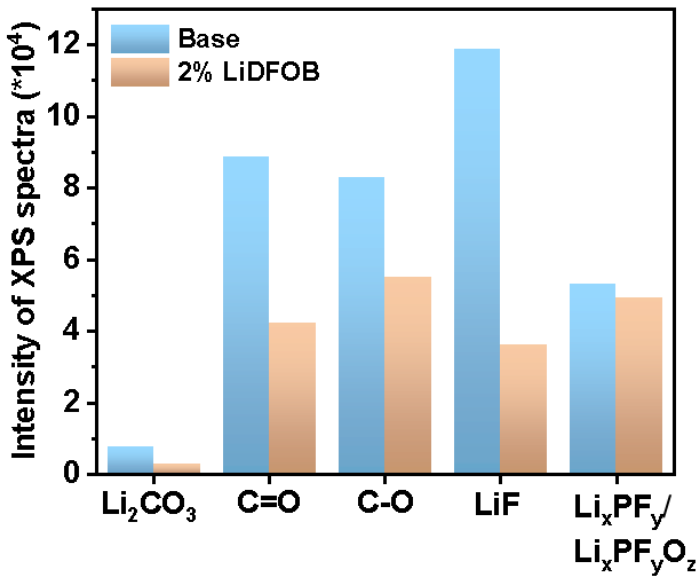

Supplementary Figure 2. The peak intensity of Li_2CO_3, C=O, C-O, LiF, and $Li_xPF_y/Li_xPF_yO_z$ on the cycled Li anode surface in base and LiDFOB-containing electrolyte.

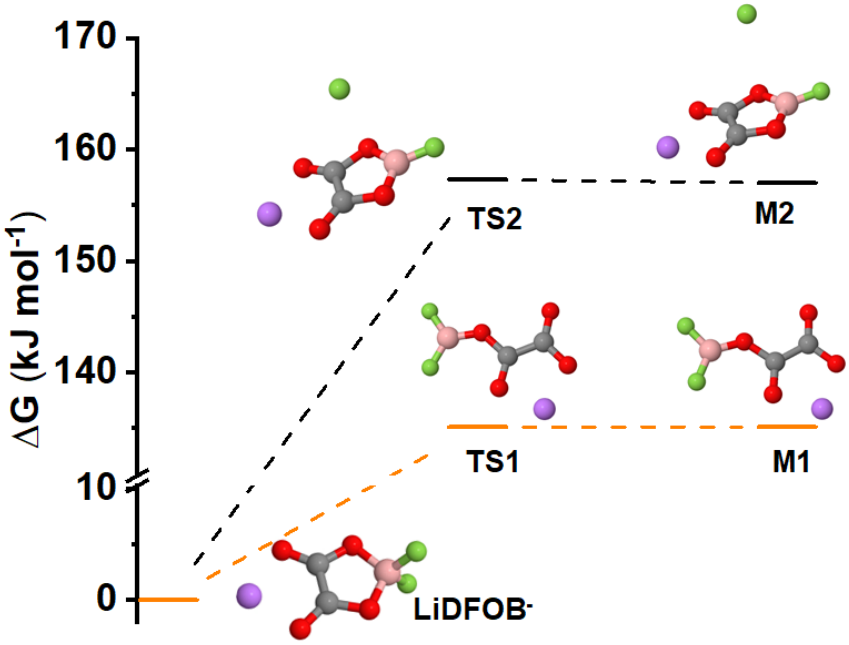

Supplementary Figure 3. Optimized structures in two possible reaction pathways for the reduction decomposition of $LiDFOB^-$ and relative Gibbs free energy (ΔG) of all stationary points.

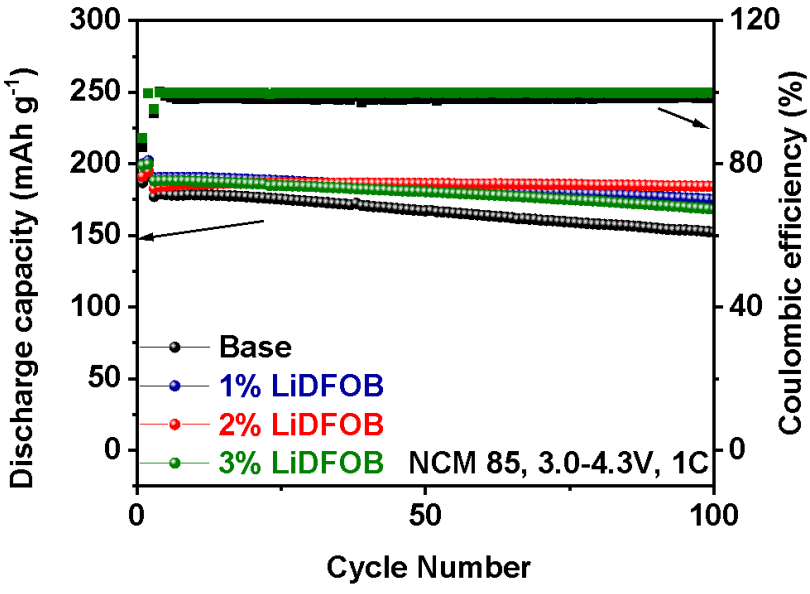

Supplementary Figure 4. Cycling performance of the batteries at 1 C in the voltage range of 3.0-4.3 V at electrolytes with 0 wt%, 1 wt%, 2 wt%, and 3 wt% LiDFOB additive.

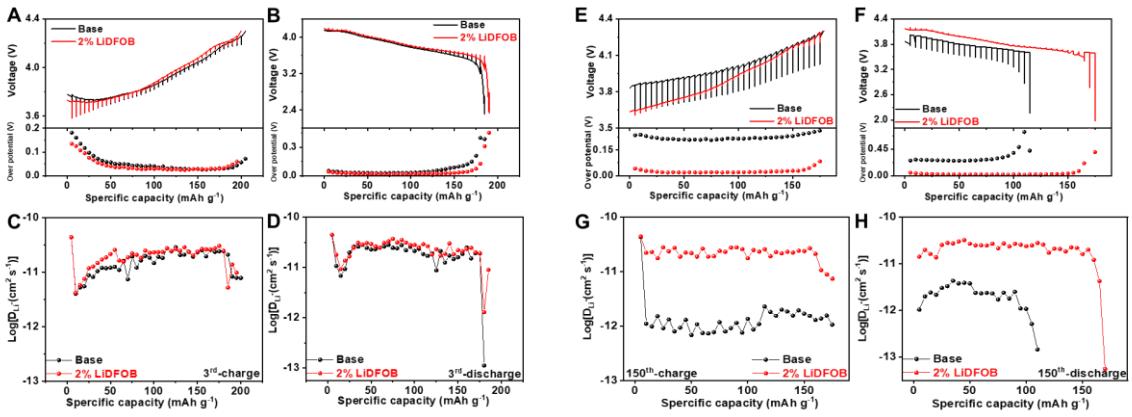

Supplementary Figure 5. (A&B, E&F) The GITT curves, calculated over potential and (C&D, G&H) Li^+ diffusion coefficient of NCM85 electrodes: charging after (A, C) 3 cycles and (E, G) 150 cycles, discharging after (B, D) 3 cycles and (F, H) 150 cycles.

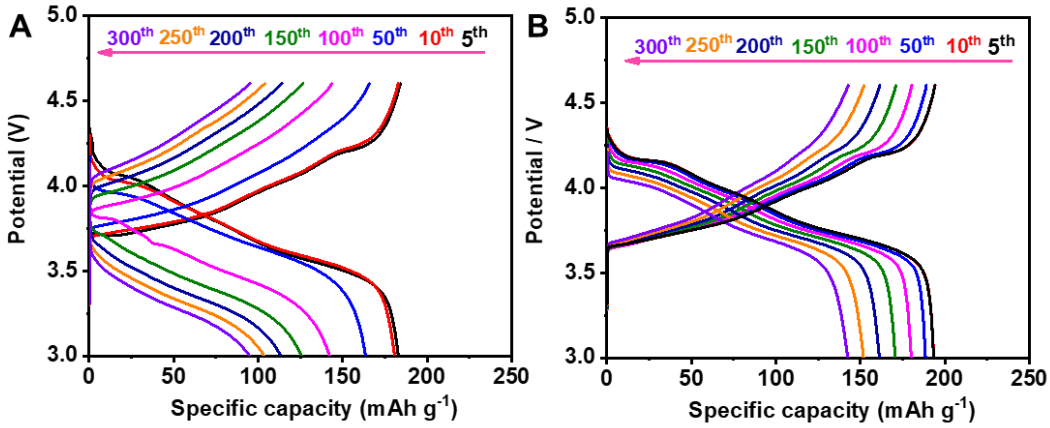

Supplementary Figure 6. Charging/discharging curves of Li||NCM85 batteries with (A) base electrolyte and (B) LiDFOB-containing electrolyte at different cycles in the voltage range of 3.0-4.6 V.

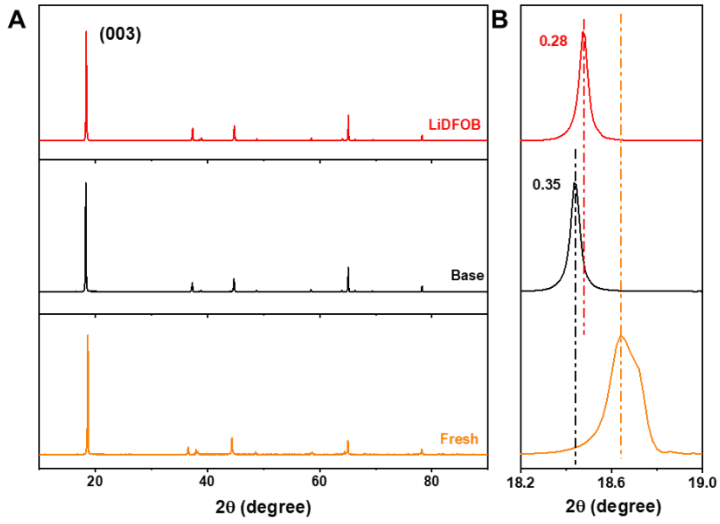

Supplementary Figure 7. Ex-situ XRD patterns of fresh and cycled NCM85 electrodes after cycling at different electrolytes: (A) full range and (B) the enlarged patterns of 18.2 º- 19 º.

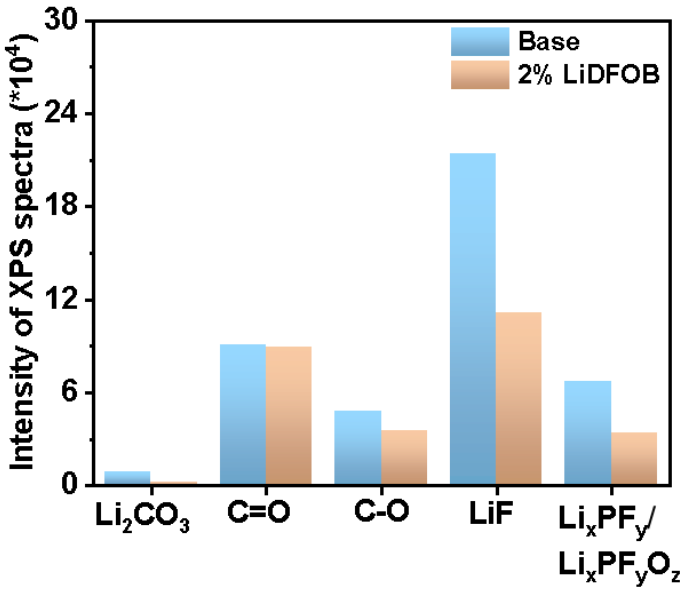

Supplementary Figure 8. The peak intensity of Li_2CO_3, C=O, C-O, LiF, and $Li_xPF_y/Li_xPF_yO_z$ on the cycled NCM85 cathode surface in the base and LiDFOB-containing electrolyte.

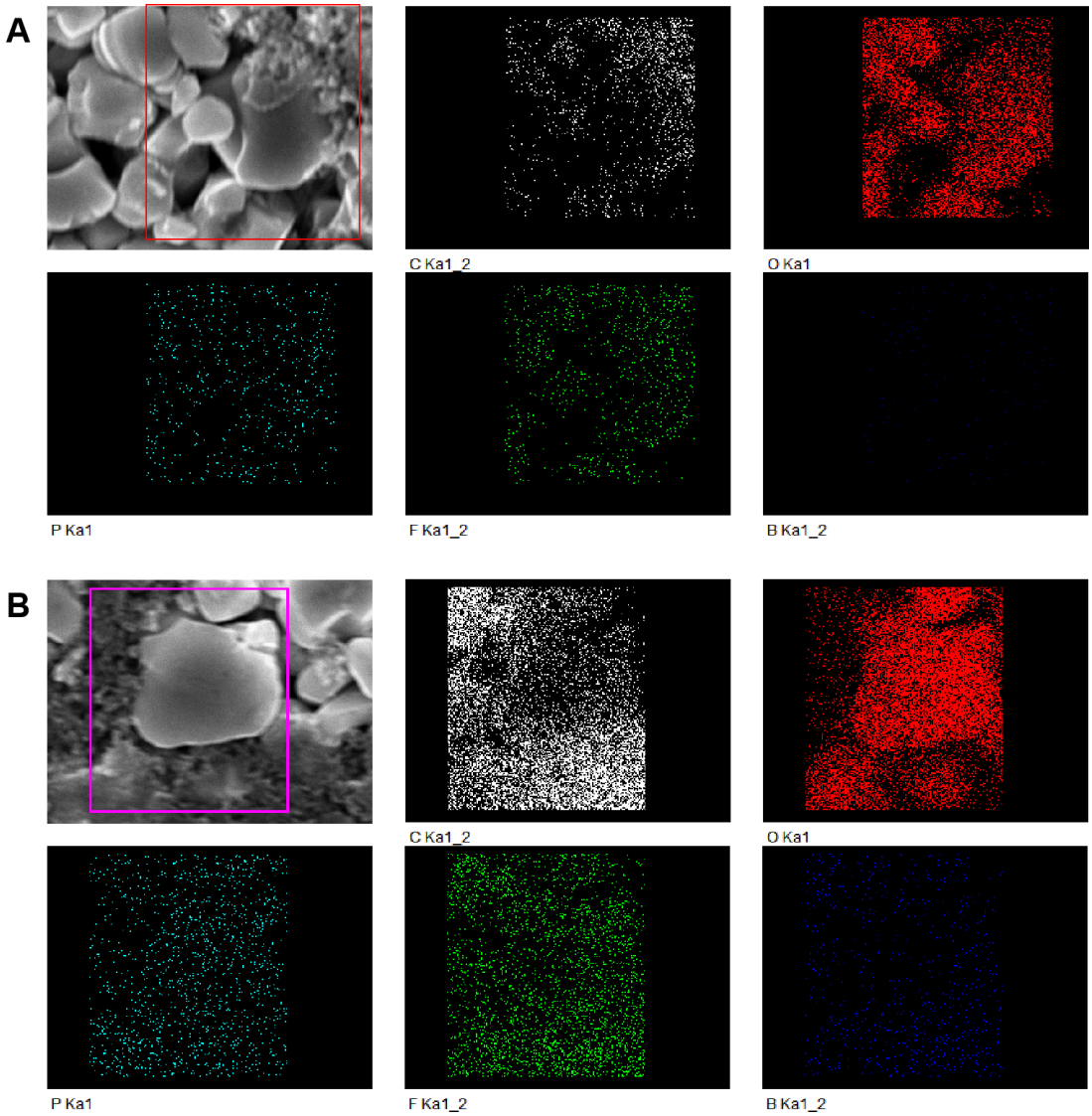

Supplementary Figure 9. The SEM and EDS-mapping of NCM85 cathode cycled in (A) base electrolyte and (B) LiDFOB-containing electrolyte.

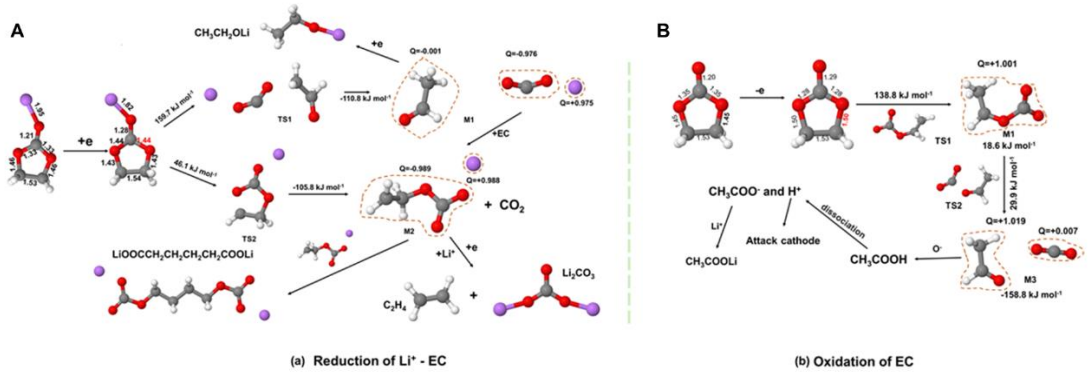

Supplementary Figure 10. (A) Possible reductive and (B) oxidative decomposition mechanism of EC, together with the reaction energy (kJ mol^{-1}).

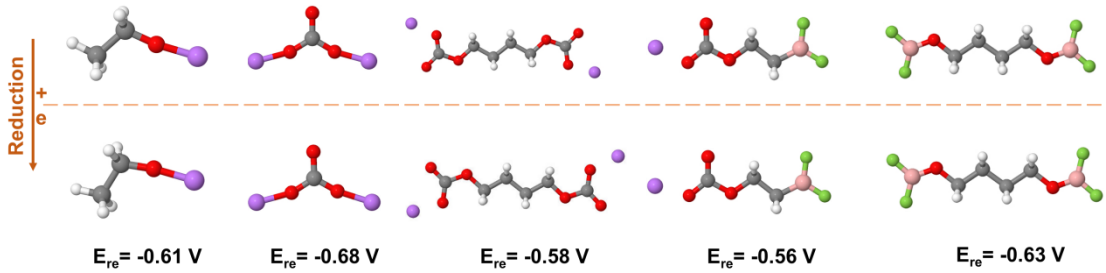

Supplementary Figure 11. The reduction potential of CH_3CH_2OLi, Li_2CO_3, LEDC, $BF_2CH_2CH_2COOLi$, and $BF_2OCH_2CH_2CH_2CH_2OBF_2$.

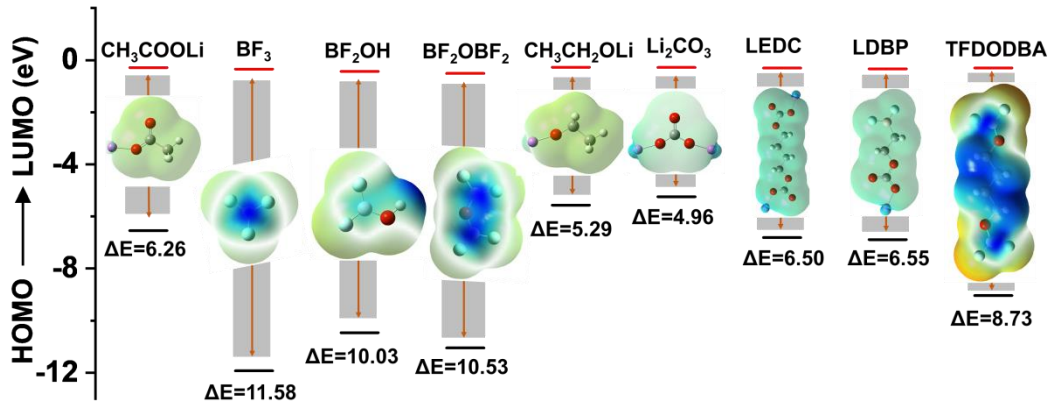

Supplementary Figure 12. The LUMO-HOMO energy levels of CH_3COOLi, BF_3, BF_2OH, BF_2OBF_2, CH_3CH_2OLi, Li_2CO_3, LEDC, LDBP, and TFDODBA.

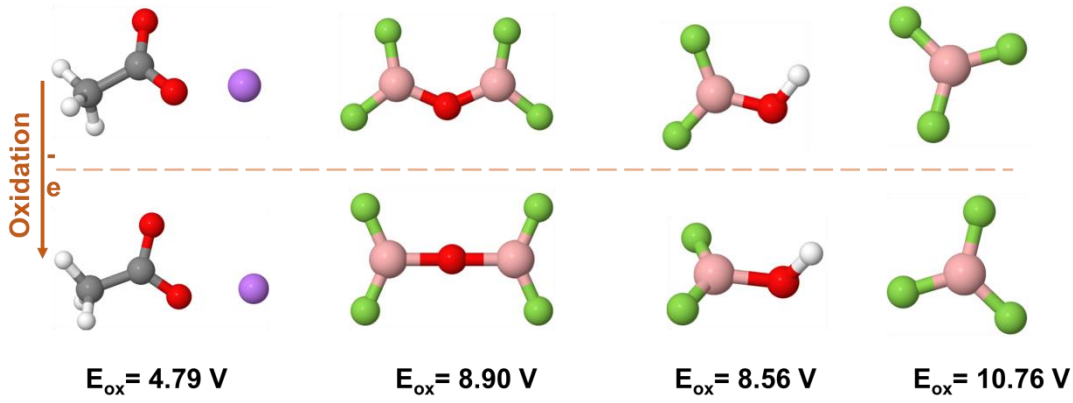

Supplementary Figure 13. The oxidation potential of CH_3COOLi, BF_2OH, BF_2OBF_2, and BF_3.

Supplementary Table 1. The fitting results of ohmic impedance (R1), interfacial impedance (R2), and charge transfer impedance (R3) of the cycled lithium metal anode of Figure 2F.

Electrolyte	R1	R2	R3
Base	96.41	54.03	8.21
Base+2 wt% LiDFOB	87.1	45.82	6.65

Supplementary Table 2. Summary of electrochemical performance of the NCM(Ni ⩾80 %) with different electrolyte additives at the high cutoff voltage of over 4.6 V

Cathode	Electrolyte composition	Current density (1C=200 mAh g^{-1})	Voltage range (V vs. Li^+/Li)	Capacity retention	Capacity promotion rate	Rate capacity	Ref.
NCM811	1 M $LiPF_6$ and 0.2 M LiDFOB in FEC/ EMC/TFA (1:3:1 v/v).	0.5 C	2.8-4.6	81.4 % after 200 cycles	15.2 %	154.5 mAh g^{-1} at 5 C	[1]
SC-NCM88	1.0 M $LiPF_6$ in EC/EMC/DEC (1:1:1 v/v) with 2wt% TCEB	1 C	2.75-4.7	80 % after 150 cycles	23.9 %	~165 mAh g^{-1} at 5 C	[2]
SC-NCM811	LiFSI/ 1.6Cl-DEE/3TTE (in molar ratio)	1 C	2.8-4.7	95.7 % after 60 cycles	-	-	[3]
NCM811	1 M LiFSI in EMC/FEC, with 3wt% UPyMA	0.5 C	2.8-4.7	80.4 % after 500 cycles	12.6 %	122.3 mAh g^{-1} at 2.5 C	[4]
NCM811	1M LiFSI in DMTMSA	0.5 C	3-4.7	88.1 % after 100 cycles	22 %	186 mAh g^{-1} at 2 C	[5]
NCM76	1 M $LiPF_6$ in EC/EMC (3:7, wt%) with 1wt% LiDFP	C/3	2.8-4.8	97.6 % after 200 cycles	20.37 %	-	[6]
SC-NCM85	2wt% LiDFOB in $LiPF_6$(EC/EMC=3: 7, wt%)	1C	3-4.6	93 % after 100 cycles	16 %	175.6 mAh g^{-1} at 10 C	This work
				84 % after 200 cycles	22 %		
				74 % after 300 cycles	22 %		

Capacity promotion rate: the value of increment in the capacity retention rate of the modified electrolyte compared to that of the base one.

Supplementary Table 3. Fitted R_f and R_{ct} values of Figure 4H and I.

Electrolyte	Cycle number	R_f	R_{ct}
Base	0.5	41.43	238.4
	300	214.2	11075
Base+2 wt% LiDFOB	0.5	63.59	159.2
	300	110.8	1115

REFERENCES

1. Q Zhao, Y Wu, Z Yang, et al., A fluorinated electrolyte stabilizing high-voltage graphite/NCM811 batteries with an inorganic-rich electrode-electrolyte interface. *Chemical Engineering Journal,* 2022. **440**. [DOI: https://doi.org/10.1016/j.cej.2022.135939]
2. F Liu, Z Zhang, Z Yu, et al., Bifunctional nitrile-borate based electrolyte additive enables excellent electrochemical stability of lithium metal batteries with single-crystal Ni-rich cathode at 4.7 V. *Chemical Engineering Journal,* 2022. **434**. [DOI: https://doi.org/10.1016/j.cej.2022.134745]
3. L Tan, S Chen, Y Chen, et al., Intrinsic Nonflammable Ether Electrolytes for Ultrahigh-Voltage Lithium Metal Batteries Enabled by Chlorine Functionality. *Angew Chem Int Ed Engl,* 2022. **61**(32): p. e202203693. [DOI: https://doi.org/10.1002/anie.202203693]
4. Z Li, J Fu, S Zheng, et al., Self-Healing Polymer Electrolyte for Dendrite-Free Li Metal Batteries with Ultra-High-Voltage Ni-Rich Layered Cathodes. *Small,* 2022. **18**(17): p. e2200891. [DOI: https://doi.org/10.1002/smll.202200891]
5. W Xue, M Huang, Y Li, et al., Ultra-high-voltage Ni-rich layered cathodes in practical Li metal batteries enabled by a sulfonamide-based electrolyte. *Nature Energy,* 2021. **6**(5): p. 495-505. [DOI: https://doi.org/10.1038/s41560-021-00792-y]
6. S Tan, Z Shadike, J Li, et al., Additive engineering for robust interphases to stabilize high-Ni layered structures at ultra-high voltage of 4.8 V. *Nature Energy,* 2022. **7**(6): p. 484-494. [DOI: https://doi.org/10.1038/s41560-022-01020-x]